Warping Nodal Levels Via M-Rep Based Diffeomorphism

Rohit R. Saboo rohit@cs.unc.edu
Sarang Joshi sjoshi@unc.edu
Joshua H. Levy levy@cs.unc.edu
Stephen M. Pizer pizer@cs.unc.edu
Julain Rosenman julian_rosenman@med.unc.edu
Medical Image Display and Analysis Group
The University of North Carolina at Chapel Hill

Abstract

The identification of lymph node drainage levels in the neck from CT scans is necessary for the proper treatment of cancer of the head and neck with radiation therapy. However, to comply with the guidelines one must segment at least 20 fiducial anatomic objects on each side, and then apply complex rules to determine six boundaries for each of nine different levels. To reduce physician time and standardize results it is necessary to automate the entire process. In this paper, we propose solving this problem by deforming the nodal levels from an atlas patient to target patient in a way combining two novel ideas: a) The large deformation diffeomorphic transformations of curved landmark paths; b) a scheme provided by m-reps and their geodesic paths for producing curved paths between corresponding points associated with the fiducial objects. This method is applicable to a wide variety of problems of mapping between an atlas and a target image with automatically segmentable structures.

1. Introduction

The medical problem that we face requires us to extract a treatment region from a 3D image, where the region is not directly segmentable via the image intensities but rather has to be inferred from other structures that can be segmented. In this paper, the treatment region is a lymph node level in the head & neck, and the anatomic structures from which it is to be inferred are many and are densely packed. The methods described in this paper then consist of the following two, applied in order.

1. A means of extracting deformation paths between an atlas and a target image for boundary points on the segmentable structures;
2. A means of diffeomorphically interpolating these deformation paths from the specified points to the part of the space in the atlas forming the unsegmentable treatment region.

2. The Medical Problem

There are approximately 40,000 cases of cancers of the head and neck diagnosed each year in the United States. These tumors are usually sensitive to radiation and chemotherapy and are often treated with both modalities. For these patients the major morbidity (treatment complication) is xerostomia, or dry mouth, which can be permanent. Xerostomia can lead to dental problems and poor nutrition, and thus a substantial decrease in the quality of the patient's life. A major breakthrough in the treatment with radiation therapy occurred about 10 years ago when it was learned how to redirect radiation dose within a patient by physically modulating the radiation beams. This technique, now called intensity modulated radiation therapy, or IMRT, can reduce the radiation dose given to the salivary glands during radiation therapy for head and neck cancer. The development of an IMRT treatment plan for a patient puts a great burden on the radiation oncologist, the physician overseeing the treatment. First, dozens of normal structures within the head and neck need to be identified and carefully outlined on each CT slice. This needs be done because the use of IMRT to push dose out of the salivary glands will necessarily increase the dose elsewhere and the dose tolerance of other organs such as the eyes, spinal cord, larynx and mandible (jawbone) must be respected. In addition, of course, the salivary glands themselves must be identified. Next, the gross tumor volume (GTV) as seen on the CT scan, or felt during the patient examination, is outlined on each CT slice. However, the GTV is not the entire target of the treatment. Head and neck cancer is notorious for spreading invisibly into neighboring structures and down lymphatic pathways in complicated ways. This spread cannot be seen because it is microscopic, but if left untreated it will often serve as a

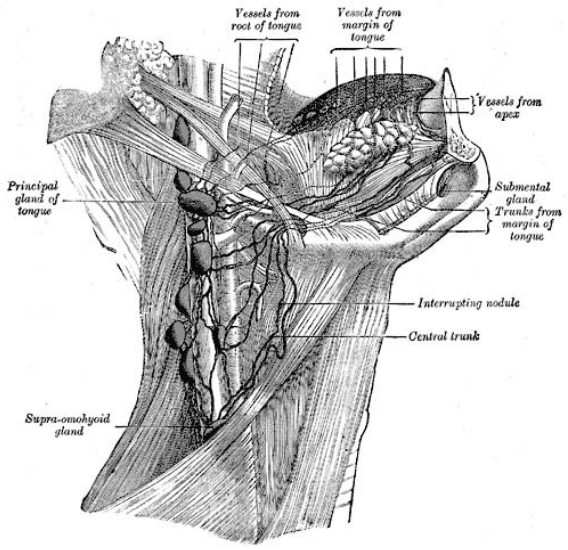

Figure 1. Lymphatics of the head and neck

Figure 2. Three different nodal levels on a CT scan

nidus of relapse. Determining this larger clinical target volume, or CTV, which includes the GTV plus the microscopic spread is a major task for the radiation oncologist.

Fig. 1, which has been obtained from Gray's anatomy 1918, shows a schematic of the lymphatic pathways in the head and neck, but as it is only a two-dimensional drawing, the full complexity of the lymphatic pathways (and thus the potential CTV) is not appreciated. To simplify the situation, lymph node chains are collected into treatment regions called levels depending on their surgical accessibility and susceptibility to tumor spread from different tumor sites. Fig. 2 illustrates the distribution of some of the levels on a given CT slice. Drawing these nodal levels on each slice according to the official rules [5] is very difficult. The rules indicate how the regions are related to at least twenty anatomic structures on each side and, in our experience,

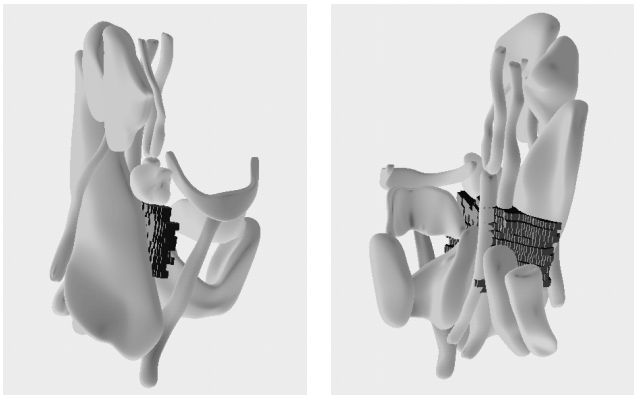

(a) Anterior view (b) Posterior view

Figure 3. Some of the segmented head and neck organs with the Level-III nodal region

many more than that. We call these the *fiducial* structures. Thus drawing the nodal levels specifically requires the segmentation of all these structures.

In this paper, we focus on the nodal treatment region called Level-III, which is shown in the form of a block of charcoal-colored voxels in fig. 3, for our tests. These Level-III nodal levels have been segmented along with ten neighboring fiducial organs, which are needed to help in identifying them, from two different patients. These organs include the hyoid bone, carotid arteries, scalene muscles, thyroid, thyroid cartilage, and others.

3. The Image Analysis Approach

We presume that we can define an anatomic atlas in which the fiducial structures and the treatment region are defined. The chief idea is to interpolate the transformation describing the deformation of the objects in the atlas to the target patient, into deformation on the treatment region. We propose to use m-reps, one from the atlas and the other from the target patient, as the basis for deriving a correspondence on the m-rep implied boundaries of the objects. The geodesic paths that give the shortest distance between m-reps yield a curved path for each boundary point. These curved paths can then be leveraged to produce a diffeomorphic deformation on the nodal levels following the theory of large deformation diffeomorphic transformation of landmark data developed in [11]. The use of inter-m-rep geodesic paths in this way, and producing a diffeomorphism given landmark paths are novel.

The m-rep models and their conformation in the atlas and their segmentation from the target image are not the subject of this paper. The models have been developed for the fiducial structures with the help of previously described methods of multi-object fitting of m-rep models to manual seg-

mentations from training images [13]. These training models yield a probability density on geometric models as well as a probability density on intensity histograms in model-relative regions [2]. The segmentation in a target image operates by posterior optimization using these probability densities [15].

4. Previous Work

Bookstein [1], Dryden [9], Rueckert [18], Joshi [14], Lorenzen [12], Grenander [6], among many others, have developed an approach of deforming a treatment region by keeping an *atlas*, which contains a *mean segmentation* of the structures over a sizable population and computing deformations from that atlas. However, the methods cannot simultaneously a) automatically produce the correspondences between the atlas and a target image, b) automatically compute extensive deformation to a target image, and c) produce deformations that can be guaranteed to be diffeomorphic.

The method of segmentation via posterior optimization of m-reps has been shown to have hope for automatic extraction of multi-object complexes [2]. In this paper, we take this debatable point as a premise. The work on m-reps has included much on developing m-rep models for various structures of the body [17]. These include many of the head & neck structures that are the target of this paper.

Moreover, Fletcher et. al [3] have shown how to produce shortest distance diffeomorphic transformations on the interior of regions represented by m-reps. The method leverages the fact that m-reps carry with them unique object-relative coordinates for the interior of each m-rep [16].

However, m-reps fail to model the interstitial regions favorably. The Level-III nodal region is an interstitial region. This fact, coupled with its peculiar geometry makes it unsuitable for direct segmentation by deformable m-reps, and thus makes it unsuitable as a means of directly providing its deformation via m-reps techniques.

We propose instead to transfer the deformation of the anatomic objects that can be represented by m-reps to the treatment region. We leverage the ideas developed for large deformation, landmark diffeomorphic transformations via flows to transfer the treatment region into the image of the target patient.

Thin plate splines have been used previously to deform segmented structures from the image of one patient or an atlas to another. However, typically a person has to manually define the landmarks in the atlas and carry them over to the target case. When the variability is small, thin plate splines work just fine. However, as the variability increases, one can get folding, i.e., a non-diffeomorphic warp.

Image-based and landmark-based diffeomorphisms have been achieved by the fluid registration framework described in Miller, Joshi, et. al [14]. This method has been shown to be successful while dealing with the structures in the brain and same-patient inter-day male prostate [4]. However, when dealing with the inter subject brain structures, the use of manually placed landmarks has been found necessary [10]. The main contribution of this method brought forth the idea that diffeomorphic paths are curved space-time trajectories and that these paths can be generated via integration of a sequence of velocity vector fields.

One of the contributions of this paper is that if there are a collection of non-intersecting curved space-time paths available between the atlas and target, then a diffeomorphic transformation between the atlas and the target can be computed by integrating a spline interpolation of the velocities defined along the path. However, this still leaves the question of how to obtain such a suitable path. In previous work on diffeomorphic landmark matching [7] the paths were estimated by minimizing an energy on the velocity fields with the constraints that the paths begin and end at the given landmark points. In this paper, we use the paths generated by the continuous Geodesic interpolation of two m-rep models.

The next section describes the m-rep-relative *figural* coordinates that provide correspondence between points on m-reps in the atlas and m-reps for the same fiducial structures segmented from the target image. Then there follows a section on the production of curved paths via geodesics between the corresponding m-reps. The succeeding section briefly describes the generation of diffeomorphic transformations given space-time landmark trajectories.

4.1. M-reps

An m-rep is a specialization of the Blum medial axis representation. Any anatomic object can be approximated by a small collection of *figures*, each with a non-branching medial manifolds (axes). Each medial manifold can be con-

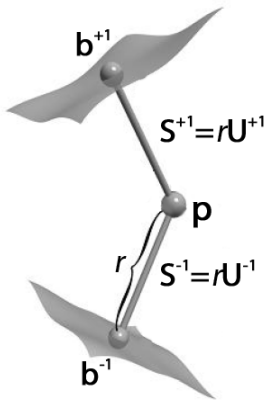

Figure 4. A medial atom.

Figure 5. An m-rep model of the Medial Scalene muscle showing the grid of medial atoms.

sidered as a continuum of hubs symmetrically placed with respect to the object boundary. From each hub there extend two equal length vectors called *spokes*, which end at and are orthogonal to two implied boundary points. The hub and its two associated spokes are known as a *medial atom*. The medial atom, as shown in fig. 4, is represented by the 4-tuple $\left(\mathbf{x}, r, \mathbf{U}^{-1}, \mathbf{U}^{+1}\right)$, where $\mathbf{x} \in \mathbb{R}^3$ is the position of the hub, $r \in \mathbb{R}^+$ is the common spoke length, and $\mathbf{U}^{-1}, \mathbf{U}^{+1} \in S^2$ are the two spoke directions. These two spoke directions give us two opposing points on the surface $\mathbf{b}^{-1}$ and $\mathbf{b}^{+1}$, known as the *implied boundary points*. The normals to the surface at these points are given by $\mathbf{U}^{-1}$ and $\mathbf{U}^{+1}$ respectively.

A discrete m-rep is formed by sampling the medial manifold over a spatially regular grid. In the implementation we used, for ordinary three dimensional objects, the grid (fig. 5) is of the form of a rectangular mesh of medial atoms $\mathbf{m}_{ij}$, where $i \in [1, m]$ and $j \in [1, n]$. The curious reader is referred to Pizer et. al [16] for a much more detailed discussion on m-reps.

4.2. Figural coordinates and inter-object correspondence

The m-rep mesh is considered to represent a continuous sheet of atoms with non-crossing spokes, which imply a closed figural boundary surface. This continuous sheet is obtained by interpolating the grid and is parameterized by $(u, v) \in [(j, j+1) \times (k, k+1)]$ for the part of the mesh with the m^{th}_{jk} atom at its lower left corner.

Methods for atom interpolation are described in Thall [19]. The result of this interpolation is that every surface point can be assigned a figural coordinate $[u, v, \phi]$. The parameter ϕ indicates the side ($-\pi/2$ or $+\pi/2$), and $\phi \in (-\pi/2, +\pi/2)$ around the crest. The parameters (u, v) are taken from the interpolated atom which corresponds to this surface point. The subdivision is done finely enough, so that each the surface can be represented by a set of voxel-size tiles.

These coordinates can be extended to give unique, object-relative coordinates for the whole region interior to the implied boundary. Every point (x, y, z) in this region can be assigned a figural coordinate (u, v, ϕ) and τ, where τ is a measure of distance from the hub along the spoke in terms proportional to r. τ is 0 at the hub and 1 at the implied boundary.

Not only do figural coordinates provide a very natural way to parameterize the object surface, but also these coordinates yield a natural correspondence between different variants of the same figure. As the model deforms, i.e., the parameters making up the 4-tuple $\mathbf{m}_{ij}$ change, the surface points change their physical position in (x, y, z) space. However, they carry over the same figural coordinates. Let us compare the thyroids between two patients. If we fit an m-rep to one thyroid and then deform the model and fit it to the second thyroid, then we can easily identify corresponding positions on the two thyroids using this figural coordinate system. Fig 6 shows the correspondence for points on the surface of a kidney. *Thus, we have a natural set of landmarks provided by the m-reps and their figural coordinates.*

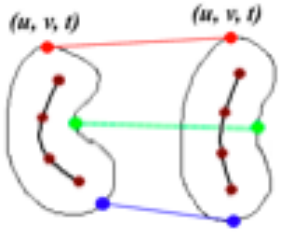

Figure 6. Correspondence between points on the surface of two different objects.

4.3. Geodesics between m-reps

M-reps lie in a *Riemannian symmetric space* space. Every point in this space is an m-rep. Thus, stepping along any smooth curve in this space yields a continuously varying m-rep model. Each point in this space is also associated with a tangent space $T_x(M)$ and a *Riemannian metric*, a smoothly varying inner product on this tangent space. It suffices to say here that a *geodesic curve* is a special curve, which minimizes the *distance* between the two m-reps, which forms its end-points. This distance is also known as the *geodesic distance* or the *Riemannian distance*. The interested reader is referred to [8] for an in-depth study of Riemannian symmetric spaces.

For any tangent vector $v \in T_xM$, there exists a unique geodesic, $\gamma_v(t)$, v being its initial velocity. The *Riemannian exponential map*, maps v to the point at $t = 1$ along the geodesic γ_v. Note, that the geodesic has a varying velocity but a constant speed given by $|| \left[\frac{d\gamma_v}{dt}\right]_t || = ||v||$. Thus the exponential map, $Exp_x(v)$, preserves distances from the initial point, i.e., $d(x, Exp_x(v)) = ||v||$. In the neighborhood of zero, the exponential map is a diffeomorphism. The inverse in this neighborhood is known as the *Riemannian log map*, which is denoted as $\log_x$. Thus for a point y in the neighborhood of x, the geodesic distance between them is given by $d(x, y) = ||\log_x(y)||$.

We can march along the geodesic between two m-reps by marching along the geodesics between the corresponding pairs of medial atoms $\mathbf{m}_1 = (\mathbf{x}_1, r_1, \mathbf{U}_1^{-1}, \mathbf{U}_1^{+1})$ and $\mathbf{m}_2 = (\mathbf{x}_2, r_2, \mathbf{U}_2^{-1}, \mathbf{U}_2^{+1})$. A medial atom $\mathbf{m}(t)$ that is fractional distance t along the geodesic between $\mathbf{m}_1$ and $\mathbf{m}_2$ is given by

$$\mathbf{m}(t) \quad = \quad Exp_{\mathbf{m}_1}\left(t \log_{\mathbf{m}_1}(\mathbf{m}_2)\right).$$

The Exponential and Log maps for the manifold of medial atoms $M(1)$ are nothing but the direct product of the maps of the individual components. Thus, we have

$$\begin{aligned}\mathbf{m}(t) &= (\mathbf{x}_1 + t(\mathbf{x}_2 - \mathbf{x}_1), \\ &\quad e^{\log(r_1)+t(\log(r_2)-\log(r_1))}, \\ &\quad Exp_{\mathbf{U}_1^{-1}}(t \log_{\mathbf{U}_1^{-1}}(\mathbf{U}_2^{-1})), \\ &\quad Exp_{\mathbf{U}_1^{+1}}(t \log_{\mathbf{U}_1^{+1}}(\mathbf{U}_2^{+1}))\Big) . \qquad (1)\end{aligned}$$

The exponential and log maps for the spoke directions apply to the sphere S^2. The geodesics at any point on the sphere are the great circles through that point. Thus, the geodesics through the point $p = (0, 0, 1)$ are the great circles through it, or in this case, the meridians. This exponential map is given by

$$Exp_p(v) = \left(v_1 \frac{sin||v||}{||v||}, v_2 \frac{sin||v||}{||v||}, cos||v||\right), \qquad (2)$$
$$where\ ||v|| = \sqrt{v_1^2 + v_2^2}.$$

The inverse mapping, i.e., the log map for a point $(x_1, x_2, x_3) \in S^2$ is given by

$$\log_p(x) = \left(x_1 \frac{\theta}{sin\theta}, x_2 \frac{\theta}{sin\theta}\right), \qquad (3)$$
$$where\ \theta = cos^{-1}(x_3).$$

4.4. Large Deformation Diffeomorphisms

Given a set of landmark points $\mathbf{x}_i$, each with a displacement d_i, traditional spline methods such as Thin Plate Splines (TPS) interpolate the displacement field to the entire volume by minimizing a differential energy defined by a linear differential operator. Although such methods have been extensively studied and used in the literature[1] a major short coming of these methods is that they do not generate diffeomorphic transformations. When the deformations between the atlas and the image under analysis are large and curved, the transformations introduce folding and do not preserve the topology of the atlas. In the head and neck application, this is precisely the case. Shown in fig. 8 is the application of the now well-known thin plate spline interpolation. Notice the folding of the nodal segmentation produced by the TPS solution. To overcome this, we use the diffeomorphic landmark mapping framework developed by Joshi and Miller [11]. In this frame work a time indexed transformation $h(\mathbf{x}, t)$ mapping the atlas to the target is defined via an integration of a velocity vector field, given by

$$h(\mathbf{x}, t) = \mathbf{x} + \int_0^t v(h(\mathbf{x}, t), t)dt\ . \qquad (4)$$

In this frame work, given a set of landmark points $\mathbf{x}_i$, each with a path $h(\mathbf{x}_i, t)$ describing the motion of the landmark point from the atlas to the target, the diffeomorphic transformation is estimated by first estimating a velocity vector field following the minimization

$$\hat{v}(\mathbf{x}, t) = \arg\min_v \int_0^1 ||Lv(\mathbf{x}, t)||^2 dt$$
$$subject\ to:\ v(h(\mathbf{x}_i, t)) = \frac{dh(\mathbf{x}_i, t)}{dt},$$

where L is a linear differential operator. Many linear differential operators have been used in the literature. In this paper, we primarily use the biharmonic thin plate spline operator. Given the complete space-time paths of the landmark points, the above minimization has a closed form solution with the velocity fields given as a superposition of Greens functions of the differential operator $LL^\dagger$ that is

$$v(\mathbf{x}, t) = \sum_{i=1}^{N} \beta_i(t) K(h(\mathbf{x}_i, t), x) + A\mathbf{x} + T\ , \qquad (5)$$

where the weights $\beta_i(t)$ and the affine motion $A\mathbf{x} + T$ are chosen so that the velocity field satisfies the constraints $v(h(\mathbf{x}_i, t)) = \frac{dh(\mathbf{x}_i, t)}{dt}$ and boundary conditions. In three dimensions, using the TPS operator and zero boundary condition at infinite, results in a Greens function $K(x, y)$ given by $\frac{1}{||x-y||}$ and the conditions

$$\begin{aligned}\sum_{i=1}^{N} \beta_i(t) &= 0\ and \\ \sum_{i=1}^{N} \beta_i(t) h(\mathbf{x}_i) &= 0\ .\end{aligned}$$

For each time t, the weights $\beta_i(t)$ can be estimated by a solution of a linear system of equations. For details see [11].

4.4.1 Discrete integration of velocity fields.

For a practical computer implementation, the continuous integral of the velocity vector fields is discretized in time as follows: Let $t_j, j = 0, \cdots, M$ be a discretization of the interval $[0, 1]$, then given a velocity field $v(x, t)$, the integral in equation 4 can be written recursively as

$$h(\mathbf{x}, t_{j+1}) = h(\mathbf{x}, t_j) + \int_{t_j}^{t_{j+1}} v(h(\mathbf{x}, t), t)dt$$
$$\text{with}\ \ t_j = \frac{j}{M}, j = 0, \cdots, M.$$

The above integral is approximated, resulting in

$$h(\mathbf{x}, t_{j+1}) = h(\mathbf{x}, t_j) + \frac{1}{M} v(h(\mathbf{x}, t_j), t_j) \,, \qquad (6)$$

with the initial condition $h(\mathbf{x}, 0) = \mathbf{x}$. Using this discretization, the generation of a large deformation diffeomorphic transformation can be seen as a repeated application of a TPS interpolation. Substituting equation 5 into equation 6 yields in a solution of a sequence of thin plate spline problems

$$\begin{aligned} \frac{h(\mathbf{x}, t_{j+1}) - h(\mathbf{x}, t_j)}{1/M} &= \sum_{i=1}^{N} (\beta_i(t_t) K(h(\mathbf{x}_i, t_j), \mathbf{x}) \\ &\quad + A_j \mathbf{x} + T_j) \,, \qquad (7) \end{aligned}$$

This can be interpreted as a repeated application of a spline interpolation for incremental small motion of the landmark along the given paths.

5. New Method: M-rep Based Diffeomorphisms

We have reasoned that the treatment region is not a suitable candidate for an m-rep model chiefly because of its peculiar geometry and interstitial nature. We have m-rep models for the structures, which define the treatment region. We have also discussed the drawbacks of the existing methods.

The basic approach, we follow here, is to obtain landmarks and their deformation paths with the help of m-rep models and then interpolate this deformation to warp the treatment region. The algorithm can be broken into the following steps, which are detailed later:

1. Obtaining the landmarks: The vertices of the treatment region are projected onto the surface of the closest m-rep. This lets us associate a figural parameter with each vertex of the tileset representing the treatment region. These back-projected points serve as the landmarks.

2. Obtaining the deformation paths: Each m-rep is moved smoothly along a geodesic from the atlas to the target patient. This gives us a smooth path for the deformation associated with each landmark.

3. Interpolate the paths to the entire volume using the large deformation diffeomorphisim frame work.

5.1. Obtaining the Landmarks

The treatment region is represented as a tileset which is made up of a number of vertices, $\mathbf{v}_{k_0}$. For each vertex, the closest point on the surface of the nearest m-rep is located. This step is referred to as the back-projection. The subdivision of the surface of the m-rep is done finely enough, so that each tile on the surface of the m-rep is of the size of a voxel or smaller.

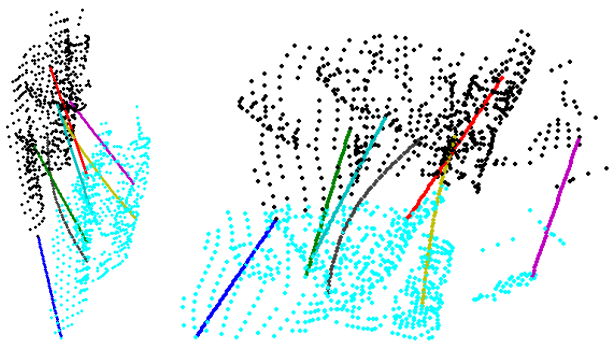

Figure 7. Deformation paths for a chosen set of landmarks in two different views. These landmarks are shown in cyan for the atlas and in black for the target patient. The deformation paths of seven landmarks have been plotted, each in a different color.

This back-projection is not guaranteed to be unique. However, for the case where the treatment region is pretty close to the m-rep boundary, the choice does not matter much. We must also note that the mapping may be many-to-one, i.e., multiple vertices of the treatment region may map to the same m-rep surface point. This is due to the discrete nature of the surface representation. These duplicates must be eliminated before we can use them in thin plate spline interpolation methods.

Thus for every vertex $\mathbf{v}_{k_0}$ in the tileset, we have a figural coordinate (u, v, τ) along with the m-rep number m. These 4-tuples $\mathbf{P}_{i_0} = (m, u, v, \tau)$ form the set of landmarks at time 0.

5.2. Obtaining the Deformation Paths and Generating diffeomorphic transformations.

The natural deformation path between two m-reps is along the shortest distance path, i.e., the geodesic between the m-reps. We can form discrete paths by the m-reps at M equal length segments of the geodesic from the atlas to the target patient. For each segment $t_j, j = 0, \cdots, M$ the surface is recomputed by applying the atom interpolation algorithm, and the Euclidean coordinates for each landmark (m, u, v, τ) are obtained. This gives us a smooth time-varying path of positions in real space for each landmark. The deformation paths for a particular set of chosen landmarks can be seen in fig 7. Call these $n * M$ positions $\mathbf{P}_i(t_j), j = 0, \cdots, M$, where M is the number of steps in the interpolation, n is the number of landmark points, and $i \in [1, n]$ identifies the landmark. At time step t_j, the velocities of the landmarks along the path can be approximated by $\frac{\mathbf{P}_i(t_{j+1}) - \mathbf{P}_i(t_j)}{1/M}$.

Given the velocity vectors along the paths, the entire ve-

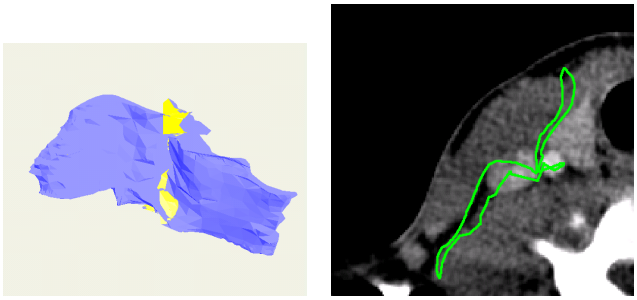

(a) 3D view (b) A single axial slice

Figure 8. The treatment region warped with TPS. In (a), the folding of the treatment region is shown by the yellow tiles.

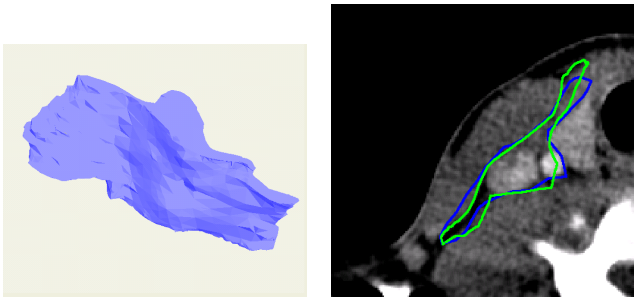

(a) 3D view (b) A single axial slice

Figure 9. The treatment region warped with the new method. In (b), the treatment region warped with the new method is shown in green, while the manually drawn one is shown in blue.

locity field for the whole image volume $v(x, t_j)$ is estimated by solving the sequence of interpolating thin plate spline problems defined by equation 7. Thus, we have

$$\frac{\mathbf{P}_k(t_{j+1}) - \mathbf{P}_k(t_j)}{1/M} = \sum_{i=1}^{N} (\beta_i(t_t) K(\mathbf{P}_k(t_j), \mathbf{P}_i(t_j)) + A_j \mathbf{P}_k(t_j) + T_j) \ . \quad (8)$$

The final transformation is computed via the recursive composition

$$h(\mathbf{x}, t_{j+1}) = h(\mathbf{x}, t_j) + v(h(\mathbf{x}, t_j))$$

In this paper as we are using the TPS operator, the above algorithm is implemented as a recursive composition of thin plate spline interpolations.

6. Results

We used the set of m-rep models and nodal levels shown in fig. 3 as the atlas. We also segmented these set of organs and the nodal level for the target patient.

We first deformed the treatment region from the atlas into the target patient with the help of TPS. To make an equitable comparison, we used m-reps for providing us with the landmarks in both the cases. For this, we computed all the landmarks as described in section 5.1. Also we computed their location on the target patient by marching along the geodesic paths. The result is shown in fig. 8. The characteristic folding problem associated with TPS over large deformations, can be seen in the form of yellow tiles in the 3D view. This folding can be seen even more clearly when we see the deformed treatment region in the form of axial slices.

Next, we deformed the treatment region from the atlas into the target patient with our new method described in the previous section. Fig. 9 shows one slice of the comparison between a manually segmented nodal level and the deformed one. The manual segmentation is shown in blue, while the deformed nodal level is shown in green. Note that while the match is not perfect, it is much better than the one obtained with TPS. Also, there is no folding. The less than perfect match is chiefly because not all the organs which define the treatment region were used for the deformation. Also, the atlas in this case comes from just one patient instead of being a mean over a large population.

7. Conclusions and Future Work

The problem of identifying the nodal levels poses many problems, some of which are quite challenging. In this paper, we have tackled the issue of deforming the nodal levels from one patient to another, given segemented m-rep models for the organs which define it.

When the deformation is small, thin plate splines can do a reasonably good job at deforming structures from one image to another. However, they need landmarks and their deformation paths as inputs. This was usually done manually. M-reps provide correspondence between several different deformations through the notion of figural coordinates. They also provide a path between these two corresponding points via geodesics. These natural landmarks and means of providing a deformation path between them can be successfully used as an input for the repetitive application of thin plate splines.

We plan to test this method further on a different set of treatment region, i.e. lymph nodal levels and also on several new patients. Also, at present, the grayscale information stored in the source and target images is never used directly. We plan to incorporate ideas from the fluid registration method, which uses grayscale information, into our method to make it more robust.

References

[1] F. L. Bookstein. *Morphometric Tools for Landmark Data : Geometry and Biology*. Cambridge University Press, 1997. 3, 5

[2] R. Broadhurst, J. Stough, S. Pizer, and E. Chaney. A statistical appearance model based on intensity quantiles. *To appear, International Symposium on Biomedical Imaging (ISBI)*, 2006. http://midag.cs.unc.edu/pubs/papers/ISBI06_Broadhurst.pdf. 3

[3] P. Fletcher, C. Lu, S. Pizer, and S. Joshi. Principal geodesic analysis for the study of nonlinear statistics of shape. *IEEE Transactions on Medical Imaging*, 23(8):995–1005, August 2004. 3

[4] M. Foskey, B. Davis, L. Goyal, S. Chang, E. Chaney, N. Strehl, S. Tomei, J. Rosenman, and S. Joshi. Large deformation 3d image registration in image-guided radiation therapy. Technical report, University of North Carolina at Chapel Hill, 2005. http://midag.cs.unc.edu/pubs/tech-rpts/Foskey05_submission.pdf. 3

[5] V. Gregoire and P. Levendag. CT-based delineation of lymph node levels and related CTVs in the node-negative neck: DAHANCA, EORTC, GORTEC, NCIC, RTOG consensus guidelines. *Radiother Oncol.*, 69(3):227–236, Dec 2003. 2

[6] U. Grenander. *Elements of Pattern Theory*. The John Hopkins University Press, June 1996. 3

[7] H. Guo, A. Rangarajan, S. Joshi, and L. Younes. Non-rigid registration of shapes via diffeomorphic point matching. In *ISBI*, pages 924–927, 2004. 3

[8] S. Helgason. *Differential Geometry, Lie Groups, and Symmetric Spaces*. Academic Press, 1978. 4

[9] I. I L Dryden and K. Mardia. *Statistical Shape Analysis*. Wiley, 1998. 3

[10] H. Johnson and G. Christensen. Consistent landmark and intensity-based image registration. *Medical Imaging, IEEE Transactions on*, 21(5):450–461, May 2002. 3

[11] S. Joshi and M. I. Miller. Landmark matching via large deformation diffeomorphisms. *IEEE Transactions on Image Processing*, 9(8):1357–1370, August 2000. 2, 5

[12] P. Lorenzen, B. Davis, and S. Joshi. Unbiased atlas formation via large deformations metric mapping. *Medical Image Computing and Computer Assisted Intervention (MICCAI)*, pages 411–418, Oct 2005. 3

[13] D. Merck, G. Tracton, S. Pizer, and S. Joshi. A methodology for constructing geometric priors and likelihoods for deformable shape models. Technical report, University of North Carolina at Chapel Hill, 2006. http://midag.cs.unc.edu/pubs/tech-rpts/Merck06_submission.pdf. 2

[14] M. I. Miller, S. C. Joshi, and G. E. Christensen. *Large Deformation Fluid Diffeomorphisms For Landmark and Image Matching*, pages 115–131. Academic Press, 1999. 3

[15] S. Pizer, P. Fletcher, S. Joshi, A. Gash, J. Stough, A. Thall, G. Tracton, and E. Chaney. A method & software for segmentation of anatomic object ensembles by deformable m-reps. *Medical Physics*, 32(5):1335–1345, May 2005. 3

[16] S. Pizer, T. Fletcher, Y. Fridman, D. Fritsch, A. Gash, J. Glotzer, S. Joshi, A. Thall, G. Tracton, P. Yushkevich, and E. Chaney. Deformable m-reps for 3d medical image segmentation. *International Journal of Computer Vision - Special UNC-MIDAG issue*, 55(2):85–106, November-December 2003. 3, 4

[17] S. Pizer and K. Siddiqi. *Medial Representations, algorithms and applications*, chapter 9. Springer, to appear. 3

[18] D. Rueckert and D. Hawkes. *3D Analysis: Registration of biomedical images.* Oxford University Press, 1999. 3

[19] A. Thall. *Deformable Solid Modeling via Medial Sampling and Displacement Subdivision*. PhD thesis, University of North Carolina at Chapel Hill, 2004. 4